The Research of Medical Science Review
ISSN: 3007-1208 & 3007-1216 Volume 4, Issue 6, 2026

PLANT-BASED COPPER OXIDE NANOPARTICLES: BIOSYNTHESIS, CHARACTERIZATION AND THEIR CLINICAL AND ENVIRONMENTAL APPLICATIONS

Hafiza Faiza[1], Khalil ur Rehman[*2], Hamza Rafeeq[3]

[1,*2,3]*Department of Biochemistry, Faculty of Engineering and Applied Sciences, Riphah International University, Faisalabad Campus, Faisalabad, Pakistan*

[*2]khalil.rehman@riphahfsd.edu.pk

DOI: https://doi.org/10.5281/zenodo.20663335

Keywords
Copper oxide nanoparticles; green synthesis; plant extract; characterization; antimicrobial activity; cytotoxicity; photocatalysis; environmental remediation

Article History
Received: 13 April 2026
Accepted: 25 May 2026
Published: 12 June 2026

Corresponding Author: *
Khalil ur Rehman

Abstract

Abstract

The growing demand for sustainable, eco-friendly nanomaterials has intensified interest in green synthesis routes for metal oxide nanoparticles. This study reports the biosynthesis, comprehensive characterization and evaluation of copper oxide nanoparticles (CuO NPs) prepared using an aqueous plant extract as a combined reducing and stabilizing agent. Synthesis parameters were optimized by response surface methodology based on a central composite design, and the optimized nanoparticles were characterized by UV-visible spectroscopy, X-ray diffraction (XRD), Fourier-transform infrared spectroscopy (FTIR), scanning electron microscopy with energy-dispersive X-ray spectroscopy (SEM-EDS), dynamic light scattering (DLS) and zeta potential analysis. Antimicrobial activity was assessed against Gram-positive (Staphylococcus aureus, Bacillus subtilis) and Gram-negative (Escherichia coli, Pseudomonas aeruginosa) bacteria by agar well diffusion and broth microdilution. Cytotoxicity was determined by MTT assay on HEK-293 and HepG2 cells, and photocatalytic performance was evaluated through degradation of methylene blue and methyl orange under visible light. The optimized conditions (18% v/v extract, 1.5 mM copper salt, 70 degrees Celsius, 90 min) yielded spherical, monoclinic CuO NPs of 30.5 +/- 2.1 nm with a narrow polydispersity index (0.18) and a zeta potential of -28.5 mV. A blue-shifted optical bandgap of 2.1 eV confirmed quantum confinement. The nanoparticles showed broad-spectrum antibacterial activity (zone of inhibition 10-24 mm; MIC 25-100 microgram/mL), dose-dependent and selective cytotoxicity (IC50 85 microgram/mL for HEK-293 and 65 microgram/mL for HepG2), and efficient photocatalytic dye degradation (92% for methylene blue and 88% for methyl orange within 180 min). These findings establish plant-mediated synthesis as a viable, environmentally benign route to functional CuO NPs with promising biomedical and environmental-remediation applications.

1. Introduction

Nanotechnology has become one of the most rapidly advancing areas of modern science, providing transformative approaches to material design across medicine, agriculture, electronics

and environmental science. The capacity to manipulate matter at the nanoscale, typically defined as dimensions between 1 and 100 nm, has created unprecedented opportunities to engineer materials with enhanced and novel functionalities (Saleem, Ejaz, Vithanage, Bolan, & Siddique, 2025). Among the nanomaterials investigated to date, metal oxide nanoparticles have attracted particular attention because of optical, electronic, magnetic and catalytic properties that differ markedly from those of their bulk counterparts (Dhir, Verma, Bhatt, Garg, & Dutt, 2023).

Copper oxide nanoparticles (CuO NPs) are especially promising owing to their favourable physicochemical properties, low cost and natural abundance relative to precious-metal nanoparticles (Naaz, Shet, & Mubarak, 2024). Because copper is an essential biological trace element, CuO NPs offer inherent biocompatibility that is attractive for biomedical use, while the semiconducting nature of copper oxide and its narrow bandgap enable efficient light absorption and photocatalytic activity for environmental remediation (Chakraborty et al., 2022).

Nanoparticles can be produced by physical, chemical or biological routes. Physical methods such as laser ablation and ball milling allow precise control of particle characteristics but require costly, energy-intensive equipment (Letchumanan, Sok, Ibrahim, Nagoor, & Arshad, 2021). Chemical methods, including sol-gel, co-precipitation and hydrothermal synthesis, offer excellent control of size and morphology but commonly rely on toxic reducing agents, organic solvents and stabilizers that pose environmental and health risks. These drawbacks have driven interest in green synthesis approaches that employ plants, microorganisms and biomolecules as reducing and capping agents (Balasubramani et al., 2025; Vijayaram et al., 2023).

Plant-mediated synthesis is particularly appealing because plant extracts are abundant, inexpensive and rich in phytochemicals such as polyphenols, flavonoids and terpenoids that act simultaneously as reductants and surface stabilizers (Yadi et al., 2018; Kumar et al., 2020). The phytochemical corona adsorbed on the nanoparticle surface can also impart additional biological activity, producing synergistic antimicrobial effects not seen with chemically synthesized counterparts (Velsankar, RM, & Sudhahar, 2020; Ijaz, Shahid, Ahmad Khan, Ahmad, & Zaman, 2017).

Despite extensive reports on green-synthesized CuO NPs, the synthesis outcome is highly sensitive to reaction variables such as extract concentration, precursor concentration, temperature, pH and reaction time, and systematic optimization is frequently lacking. Likewise, integrated studies that combine rigorous physicochemical characterization with parallel evaluation of antimicrobial, cytotoxic and photocatalytic behaviour remain comparatively scarce. The present work addresses these gaps by employing response surface methodology to optimize the plant-mediated synthesis of CuO NPs, characterizing the product with a complementary suite of analytical techniques, and systematically assessing its clinical (antimicrobial and cytotoxic) and environmental (photocatalytic) applications.

2. Materials and Methods

2.1 Materials and reagents

All chemicals and reagents were of analytical grade and used without further purification. Copper(II) sulfate pentahydrate (CuSO4.5H2O, 99.0%) served as the copper precursor; sodium hydroxide (98.0%) and hydrochloric acid (37%) were used for pH adjustment. Deionized water (18.2 MOhm.cm) from a Milli-Q system was used throughout (Tailor, Yadav, Chaudhary, Joshi, & Suvalka, 2020). Methylene blue and methyl orange were used as model dyes, the MTT reagent and DMEM/fetal bovine serum for cell culture, and Mueller-Hinton agar and broth for antimicrobial assays. Reference bacterial strains, Escherichia coli (ATCC 25922), Pseudomonas aeruginosa (ATCC 27853), Staphylococcus aureus (ATCC 25923) and Bacillus subtilis (ATCC 6633), were obtained from the American Type Culture Collection. The complete list of chemicals and the characterization instruments used are summarized in Tables 1 and 2.

Table 1. List of chemicals and reagents used.

Chemical/Reagent	Purity	Supplier
Copper(II) sulfate pentahydrate	99.0%	Sigma-Aldrich
Sodium hydroxide	98.0%	Merck
Hydrochloric acid	37%	Merck
Methylene blue	95.0%	Sigma-Aldrich
Methyl orange	85.0%	Sigma-Aldrich
MTT reagent	98.0%	Sigma-Aldrich
DMEM medium	Cell culture grade	Sigma-Aldrich
Fetal bovine serum	Cell culture grade	Sigma-Aldrich
Mueller-Hinton agar	Microbiology grade	HiMedia
Mueller-Hinton broth	Microbiology grade	HiMedia

Table 2. Equipment used for characterization.

Equipment	Model	Manufacturer
UV-Visible Spectrophotometer	UV-2600	Shimadzu
X-ray Diffractometer	D8 Advance	Bruker
FTIR Spectrometer	Spectrum Two	PerkinElmer
Scanning Electron Microscope	JSM-7600F	JEOL
Transmission Electron Microscope	JEM-2100	JEOL
Dynamic Light Scattering Analyzer	Zetasizer Nano ZS	Malvern
Centrifuge	5810R	Eppendorf
Microplate Reader	Model 680	Bio-Rad

2.2 Plant extract preparation and biosynthesis of CuO NPs

Fresh plant leaves were washed with deionized water, air-dried away from sunlight, ground to a fine powder and stored at 4 degrees Celsius. For extract preparation, 10 g of dried powder was mixed with 100 mL of deionized water and heated at 60 degrees Celsius for 30 min with continuous stirring, then filtered through Whatman No. 1 paper; the filtrate was stored at 4 degrees Celsius and used within 48 h. For synthesis, a measured volume of extract was added dropwise to copper sulfate solution under continuous stirring at the optimized temperature and pH. A colour change from blue to dark brown/black indicated CuO NP formation. The product was recovered by centrifugation at 8000 rpm for 15 min, washed three times with deionized water and twice with ethanol, dried at 60 degrees Celsius for 12 h, ground and stored for further use (Kumar et al., 2020). Synthesis was optimized using a central composite design in Design-Expert software, varying extract concentration (5-25% v/v), copper salt concentration (0.5-2.5 mM), temperature (40-80 degrees Celsius) and time (30-120 min), with particle size and antimicrobial activity as responses evaluated by analysis of variance (ANOVA).

2.3 Characterization

UV-visible spectra were recorded on a Shimadzu UV-2600 spectrophotometer (200-800 nm) after sonicating the nanoparticle dispersion for 15 min.

X-ray diffraction used a Bruker D8 Advance diffractometer with Cu K-alpha radiation (lambda = 1.5406 A) at 40 kV and 40 mA over a 2-theta range of 20-80 degrees, and crystallite size was estimated from the most intense peak using the Scherrer equation (Eren & Baran, 2019). FTIR spectra were acquired on a PerkinElmer Spectrum Two instrument (4000-400 cm-1) using KBr pellets. Morphology and elemental composition were examined by field-emission SEM (JEOL JSM-7600F, 15 kV) with energy-dispersive X-ray spectroscopy. Hydrodynamic size, polydispersity index and zeta potential were measured on a Malvern Zetasizer Nano ZS at 25 degrees Celsius (Mahdi, Yousefi, Jasim, & Salavati-Niasari, 2022).

2.4 Antimicrobial activity

Antimicrobial activity was evaluated against Gram-positive (S. aureus, B. subtilis) and Gram-negative (E. coli, P. aeruginosa) strains by agar well diffusion and broth microdilution. Bacterial suspensions matched to a 0.5 McFarland standard were spread on Mueller-Hinton agar, and 6 mm wells were loaded with CuO NP suspensions (25, 50, 100 and 200 microgram/mL); sterile water and copper sulfate served as negative and positive controls. Plates were incubated at 37 degrees Celsius for 24 h and zones of inhibition measured in millimetres (Rasheed, Bilal, Iqbal, & Li, 2017). The minimum inhibitory concentration (MIC) was determined by two-fold broth microdilution (400-3.125 microgram/mL) following CLSI guidelines, and the minimum bactericidal concentration (MBC) by subculturing wells showing no visible growth (Salayova et al., 2021).

2.5 Cytotoxicity assessment

Cytotoxicity was assessed by MTT assay on HEK-293 (human embryonic kidney) and HepG2 (hepatocellular carcinoma) cells cultured in DMEM with 10% fetal bovine serum at 37 degrees Celsius under 5% CO2. Cells seeded at 1 x 10^4 per well were exposed to CuO NPs (3.125-200 microgram/mL) for 24 h; untreated cells and 10% DMSO served as controls (Mehwish et al., 2021). After incubation with MTT and dissolution of formazan in DMSO, absorbance was read at 570 nm, viability expressed relative to control, and IC50 determined using GraphPad Prism.

2.6 Photocatalytic dye degradation

Photocatalytic activity was evaluated by degradation of methylene blue and methyl orange (20 mg/L) under visible light from a 250 W tungsten-halogen lamp with a UV cut-off filter (lambda > 400 nm). A 50 mg portion of CuO NPs was dispersed in 100 mL of dye solution and stirred in the dark for 30 min to establish adsorption-desorption equilibrium. Aliquots withdrawn at intervals were centrifuged and their absorbance measured; degradation efficiency was calculated as (C0 - Ct)/C0 x 100% (Jamzad & Kamari Bidkorpeh, 2020; Vasantharaj et al., 2021). Catalyst reusability was assessed over five consecutive cycles.

2.7 Statistical analysis

All experiments were performed in triplicate and results are expressed as mean +/- standard deviation. Statistical analysis, including ANOVA, was performed using GraphPad Prism and Design-Expert software, with $p < 0.05$ considered statistically significant.

3. Results and Discussion

3.1 Biosynthesis and optimization

The biosynthesis of CuO NPs was confirmed visually by a progressive colour change of the reaction mixture from blue (copper sulfate) through greenish-blue and dark green to a final dark brown/black, indicating nanoparticle formation through excitation of surface plasmon vibrations and bandgap transitions (Table 3).

Synthesis was optimized using a central composite design comprising 30 experimental runs. ANOVA showed that all four independent variables significantly affected both responses ($p < 0.05$). The quadratic models were significant for particle size ($F = 45.23$, $p < 0.0001$) and antimicrobial activity ($F = 38.67$, $p < 0.0001$), with non-significant lack of fit and R-squared values of 0.94 and 0.92, respectively, indicating that the models explained more than 90% of the response variation. The optimum conditions were 18% v/v extract, 1.5 mM copper salt, 70 degrees Celsius

and 90 min, predicting a particle size of 32 nm and a 18 mm zone of inhibition. Validation in triplicate gave 30.5 +/- 2.1 nm and 18.5 +/- 0.8 mm, confirming model accuracy.

Table 3. Visual observation of the biosynthesis process.

Time (min)	Colour	Observation
0	Blue	Copper sulfate solution
15	Greenish-blue	Initial reduction begins
30	Dark green	Progressive reduction
60	Brown	Nanoparticle formation
90	Dark brown/black	Complete synthesis

3.2 UV-visible spectroscopy

The UV-visible spectrum of the synthesized CuO NPs displayed a broad absorption band over 300-400 nm with a maximum at 340 nm, attributable to the characteristic bandgap transition of CuO (Figure 1, Table 4). Using the Tauc method, the optical bandgap was determined as 2.1 eV, higher than the bulk value of 1.2-1.9 eV. This blue shift reflects quantum confinement in the nanoscale regime and confirms the formation of nanosized particles.

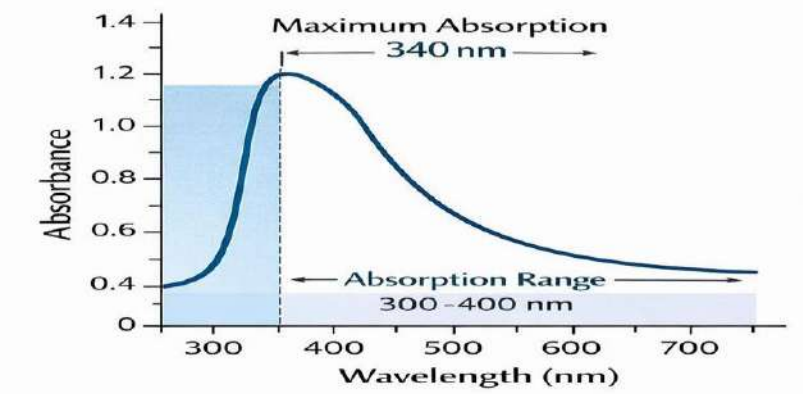

Figure 1. UV-visible absorption spectrum of biosynthesized CuO NPs showing maximum absorption at 340 nm.

Table 4. UV-Vis spectroscopy results.

Parameter	Value
Maximum absorption wavelength	340 nm
Absorption range	300-400 nm
Bandgap energy	2.1 eV
Colour in solution	Dark brown

3.3 X-ray diffraction analysis

X-ray diffraction confirmed the crystalline structure and phase purity of the nanoparticles. Distinct peaks at 2-theta values of 32.5, 35.5, 38.7, 48.7, 53.5, 58.3, 61.5, 66.2 and 68.1 degrees were indexed to the (110), (002), (111), (202), (020), (202), (113), (311) and (220) planes of monoclinic CuO, matching standard JCPDS card No. 48-1548 (Figure 2, Table 5) (Velsankar, RM, & Sudhahar, 2020). The sharp, intense peaks

indicated high crystallinity, and the absence of additional peaks confirmed a pure CuO phase free of Cu2O or other impurities. The crystallite size calculated from the (111) peak using the Scherrer equation was 28 nm, in close agreement with the DLS hydrodynamic size (Ijaz, Shahid, Ahmad Khan, Ahmad, & Zaman, 2017).

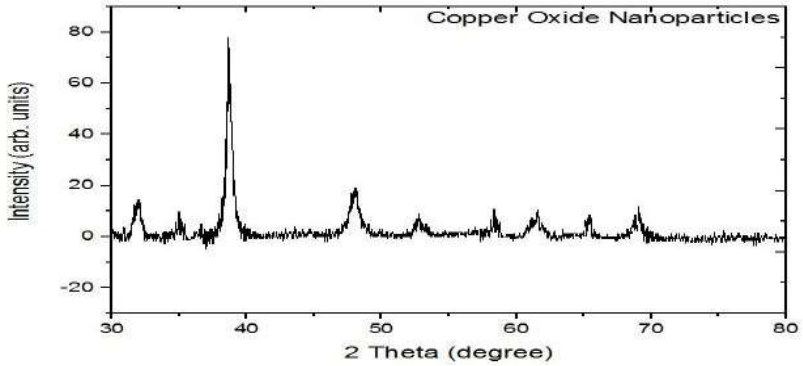

Figure 2. XRD pattern of biosynthesized CuO NPs indexed to monoclinic CuO (JCPDS 48-1548).

Table 5. XRD analysis data.

2-theta (deg)	d-spacing (A)	Miller Indices	Relative Intensity
32.5	2.75	(110)	35
35.5	2.52	(002)	55
38.7	2.32	(111)	100
48.7	1.87	(202)	25
53.5	1.71	(020)	18
58.3	1.58	(202)	20
61.5	1.51	(113)	15
66.2	1.41	(311)	12
68.1	1.38	(220)	18

3.4 FTIR spectroscopy analysis

FTIR spectroscopy identified the functional groups responsible for reduction and stabilization (Figure 3, Table 6). The band at 520 cm-1 corresponded to the Cu-O stretching vibration, confirming CuO formation. A broad band at 3400 cm-1 was assigned to O-H stretching of hydroxyl groups from adsorbed water and plant polyphenols, bands at 2920 and 2850 cm-1 to aliphatic C-H stretching, 1620 cm-1 to carbonyl C=O stretching and 1380 cm-1 to C-O stretching (Salayova et al., 2021). These organic signatures confirm that plant biomolecules were adsorbed on the nanoparticle surface, acting as capping agents.

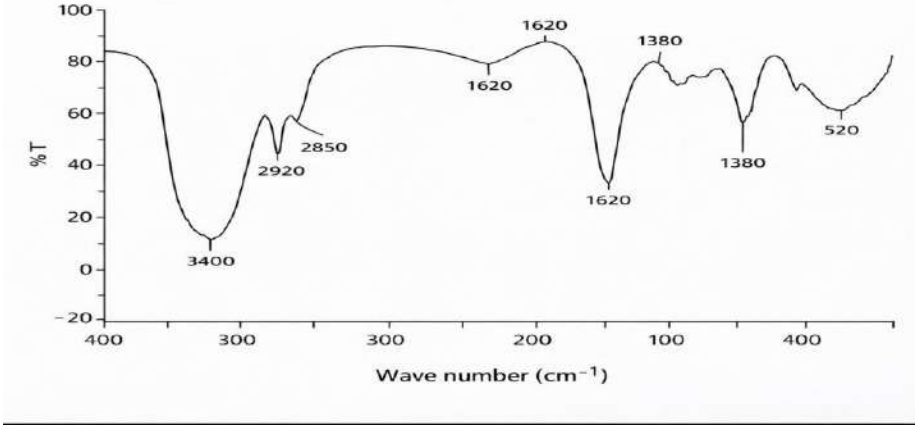

Figure 3. FTIR spectrum of biosynthesized CuO NPs showing Cu-O and plant-derived organic functional groups.

Table 6. FTIR peak assignments.

Wavenumber (cm-1)	Assignment	Source
3400	O-H stretching	Water, polyphenols
2920	C-H asymmetric stretching	Aliphatic groups
2850	C-H symmetric stretching	Aliphatic groups
1620	C=O stretching	Carbonyl groups
1380	C-O stretching	Carboxyl groups
520	Cu-O stretching	Copper oxide

3.5 SEM and EDS analysis

Scanning electron microscopy revealed predominantly spherical to quasi-spherical nanoparticles with smooth surfaces and some aggregation, with an average size of approximately 30 nm consistent with the XRD and DLS results (Figure 4, Table 7) (Pillai et al., 2020). Energy-dispersive X-ray spectroscopy showed only copper and oxygen peaks with an approximate Cu:O atomic ratio of 1:1, confirming the stoichiometry and purity of CuO without detectable contamination (Ahmad et al., 2019).

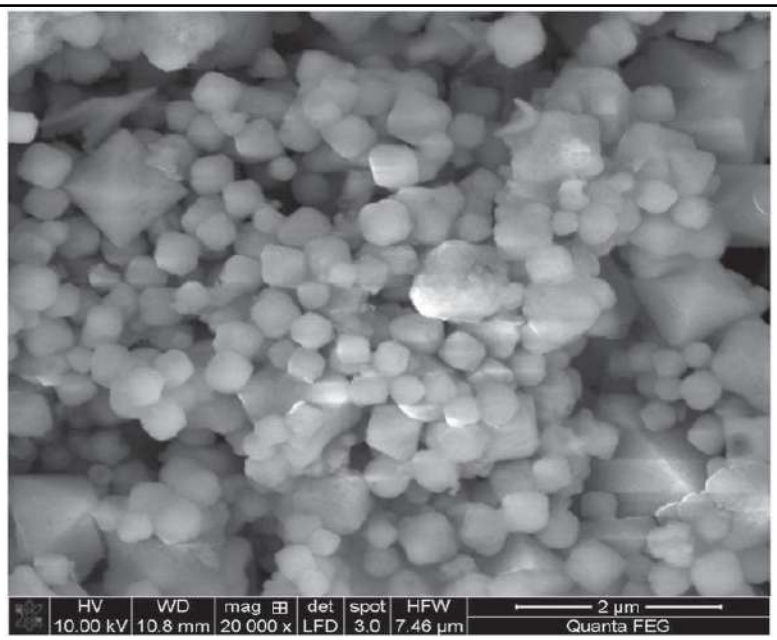

Figure 4. SEM micrograph of biosynthesized CuO NPs showing spherical to quasi-spherical morphology.

Table 7. SEM and TEM size analysis.

Parameter	Value
Morphology	Spherical/quasi-spherical
Average size (SEM)	30 nm
Average size (TEM)	28 nm
Size range	15-45 nm
Crystallinity	Polycrystalline
Lattice spacing	0.23 nm (111)

3.6 DLS and zeta potential analysis

Dynamic light scattering indicated a narrow size distribution with an average hydrodynamic diameter of 35 nm and a polydispersity index of 0.18 (Figure 5, Table 8). The slightly larger hydrodynamic size relative to the SEM and XRD values reflects the hydration layer and adsorbed phytochemical corona on the particle surface (Mahdi, Yousefi, Jasim, & Salavati-Niasari, 2022). The zeta potential was -28.5 mV; the negative charge arises from adsorbed carboxyl- and hydroxyl-bearing phytochemicals, and its magnitude above 25 mV indicates good colloidal stability through electrostatic repulsion.

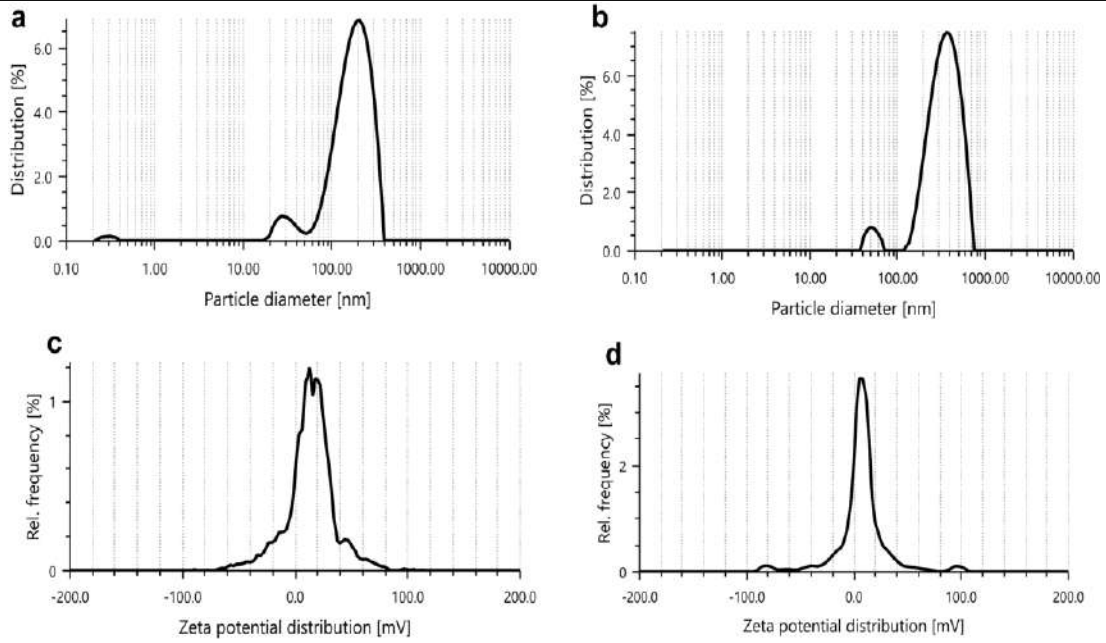

Figure 5. DLS hydrodynamic size distribution (a, b) and zeta potential distribution (c, d) of biosynthesized CuO NPs.

Table 8. DLS and zeta potential results.

Parameter	Value
Hydrodynamic diameter	35 nm
Polydispersity index (PDI)	0.18
Zeta potential	-28.5 mV
Conductivity	0.25 mS/cm
Temperature	25 deg C

3.7 Antimicrobial activity

The synthesized CuO NPs exhibited significant, dose-dependent antibacterial activity against all tested strains. In the agar well diffusion assay, zones of inhibition increased with concentration, reaching 20-24 mm at 200 microgram/mL, with Gram-positive bacteria slightly more susceptible than Gram-negative bacteria, consistent with the additional outer-membrane barrier of the latter (Figure 6, Table 9).

Broth microdilution gave MIC values of 25-100 microgram/mL, with S. aureus and B. subtilis the most susceptible (MIC 25 microgram/mL) and P. aeruginosa the least (MIC 100 microgram/mL). MBC values were generally two- to four-fold higher than the corresponding MIC values, indicating bactericidal behaviour (Figure 7, Table 10). The plant-based nanoparticles showed activity comparable to or greater than chemically synthesized CuO NPs and copper sulfate, likely reflecting synergy between copper and surface-bound phytochemicals.

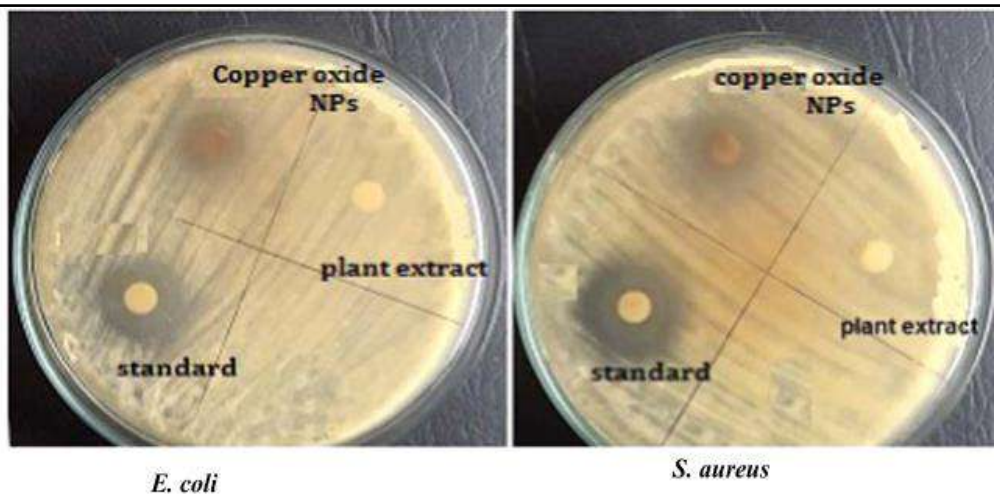

Figure 6. Zones of inhibition of CuO NPs, plant extract and standard against E. coli and S. aureus.

Table 9. Zone of inhibition measurements (mm).

Bacterial Strain	25 ug/mL	50 ug/mL	100 ug/mL	200 ug/mL
E. coli	10 +/- 1	14 +/- 1	18 +/- 1	22 +/- 1
S. aureus	12 +/- 1	16 +/- 1	20 +/- 1	24 +/- 1

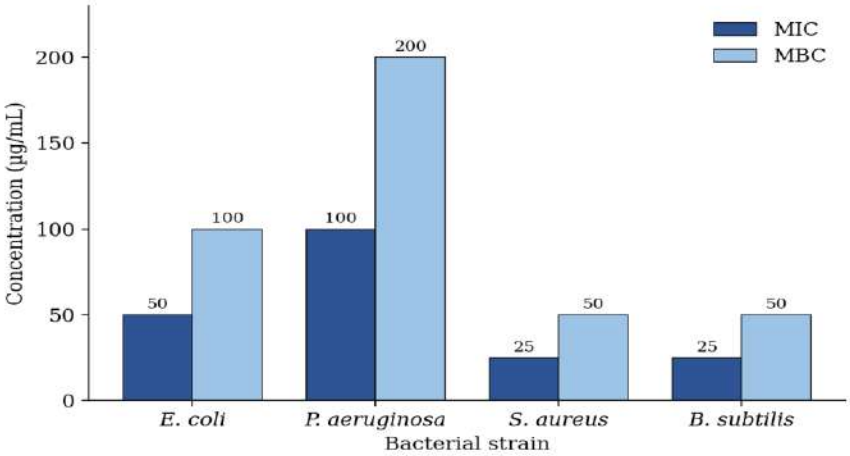

Figure 7. MIC and MBC values of biosynthesized CuO NPs against the tested bacterial strains.

Table 10. MIC and MBC values (ug/mL).

Bacterial Strain	MIC (ug/mL)	MBC (ug/mL)
E. coli	50	100
P. aeruginosa	100	200
S. aureus	25	50

Bacterial Strain	MIC (ug/mL)	MBC (ug/mL)
B. subtilis	25	50

3.8 Cytotoxicity

MTT assays demonstrated dose-dependent cytotoxicity on both cell lines (Figure 8, Table 11). HEK-293 viability remained above 80% up to 50 microgram/mL, indicating good biocompatibility at antibacterial concentrations, with an IC50 of 85 microgram/mL. HepG2 cancer cells were more sensitive, with an IC50 of 65 microgram/mL. The differential sensitivity between normal and cancer cells, together with a favourable therapeutic index relative to the MIC values, suggests potential for safe antimicrobial use and possible selective anticancer activity (Vasantharaj et al., 2021).

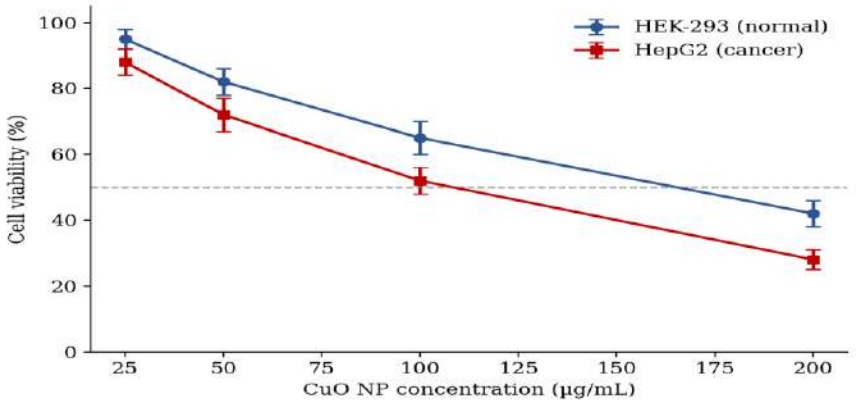

Figure 8. Dose-dependent cell viability of HEK-293 and HepG2 cells exposed to CuO NPs (MTT assay).

Table 11. MTT assay results - cell viability (%).

Cell Line	25 ug/mL	50 ug/mL	100 ug/mL	200 ug/mL
HEK-293	95 +/- 3	82 +/- 4	65 +/- 5	42 +/- 4
HepG2	88 +/- 4	72 +/- 5	52 +/- 4	28 +/- 3

3.9 Photocatalytic dye degradation

Under visible-light irradiation, the CuO NPs efficiently degraded both model dyes (Figure 9, Table 12). Approximately 92% of methylene blue was degraded within 180 min following pseudo-first-order kinetics (rate constant 0.012 min-1), compared with 88% of methyl orange (0.010 min-1). The higher efficiency for methylene blue is attributed to its cationic character favouring adsorption on the negatively charged nanoparticle surface. Reusability tests showed a gradual decline in efficiency from 92% to 78% over five cycles, indicating reasonable photocatalyst stability. The mechanism involves visible-light generation of electron-hole pairs that produce hydroxyl and superoxide radicals, which mineralize the dye molecules.

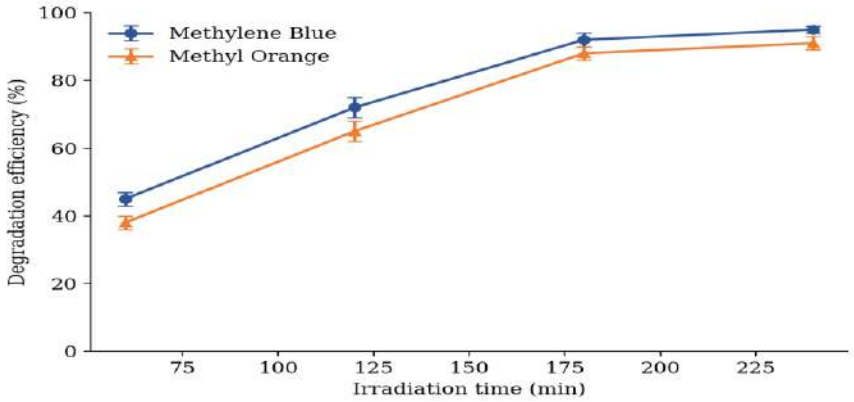

Figure 9. Photocatalytic degradation efficiency of methylene blue and methyl orange under visible light.

Table 12. Dye degradation efficiency (%).

Dye	60 min	120 min	180 min	240 min
Methylene Blue	45 +/- 2	72 +/- 3	92 +/- 2	95 +/- 1
Methyl Orange	38 +/- 2	65 +/- 3	88 +/- 2	91 +/- 2

4. Discussion

This study demonstrates the successful green synthesis of CuO NPs using plant extract as a combined reducing and capping agent. Response surface methodology proved effective for parameter optimization, yielding nanoparticles with uniform size, good colloidal stability and potent antimicrobial activity, while the complementary characterization techniques together confirmed the formation of phase-pure, crystalline, spherical CuO NPs (Garibo et al., 2020).

The average particle size of 30.5 nm aligns with the broader literature on plant-mediated metal oxide synthesis. Das, Abu-Yousef, Majdalawieh, Narasimhan, and Poltronieri (2020) reported comparable sizes near 30 nm using Moringa oleifera extract, and the narrow polydispersity index of 0.18 obtained here indicates good control over nucleation and growth under the optimized conditions, comparable to the uniformity reported by Amer and Awwad (2021). The 28 nm crystallite size from XRD was slightly smaller than the 35 nm hydrodynamic diameter from DLS, a well-documented discrepancy arising from the hydration layer and surface-bound phytochemicals; a similar offset was reported by Abdelbaky, Abd El-Mageed, Babalghith, Selim, and Mohamed (2022).

The optical bandgap of 2.1 eV represents a clear blue shift from the bulk value, consistent with quantum confinement as particle dimensions approach the exciton Bohr radius. Comparable values have been reported previously, including 2.1 eV by Baghayeri, Mahdavi, Hosseinpor-Mohsen Abadi, and Farhadi (2018) and 2.2 eV by Mousavi et al. (2018). The narrow bandgap favours visible-light absorption and underpins the strong photocatalytic activity observed here.

Antimicrobial evaluation showed broad-spectrum activity with MIC values of 25-100 microgram/mL, comparable to or better than contemporary reports. Kombaiah et al. (2018) documented MIC values of 50-100 microgram/mL for green-synthesized nanoparticles, while Kalpana and Devi Rajeswari (2018) reported enhanced activity at 25-50 microgram/mL. The greater susceptibility of Gram-positive bacteria corroborates Anju et al. (2021) and is mechanistically attributable to the absence of an outer membrane, which permits unimpeded nanoparticle access to the cytoplasmic membrane. The multimodal mechanism, encompassing membrane disruption, reactive oxygen species generation and copper-ion release, reduces the likelihood of resistance development relative to conventional antibiotics.

Cytotoxicity assessment revealed encouraging selectivity, with antibacterial concentrations exerting minimal toxicity toward normal cells. The therapeutic index derived from the IC50 (65-85 microgram/mL) and MIC (25-100 microgram/mL) values indicates a favourable safety margin, consistent with Anand, Nithiyavathi, Ramesh, Sundaram, and Kaviyarasu (2020), who reported IC50 values near 70 microgram/mL against normal cells. The enhanced sensitivity of cancer cells observed here aligns with the emerging literature on preferential cytotoxicity of metal oxide nanoparticles toward malignant cells, attributed by Hafeez et al. (2020) to the altered redox environment and elevated metabolic activity of cancer cells.

The photocatalytic performance, with 88-92% dye degradation under visible light, compares favourably with previous reports such as Arya et al. (2018) and Khan et al. (2020). The comparable or superior activity relative to chemically synthesized counterparts indicates that the phytochemical capping layer does not substantially impede photocatalysis, while the reasonable stability over five cycles, consistent with Siddiqui et al. (2018), supports potential application in wastewater treatment. Collectively, these results position plant-mediated CuO NPs as versatile nanomaterials for antimicrobial therapy and environmental remediation, providing a robust foundation for future translational research.

5. Conclusion

Plant-mediated copper oxide nanoparticles were successfully synthesized and optimized by response surface methodology, yielding spherical, monoclinic, phase-pure CuO NPs with an average size of 30.5 nm, a narrow polydispersity index of 0.18 and good colloidal stability (zeta potential -28.5 mV). The nanoparticles exhibited broad-spectrum antibacterial activity (MIC 25-100 microgram/mL) against both Gram-positive and Gram-negative bacteria, selective and dose-dependent cytotoxicity with a favourable therapeutic index, and efficient visible-light photocatalytic degradation of organic dyes (up to 92%) with reasonable reusability. These results confirm that green, plant-based synthesis is an environmentally benign and effective route to multifunctional CuO NPs with strong potential in antimicrobial therapy and environmental remediation. Future work should identify the specific phytochemicals responsible for reduction and capping, evaluate activity against multidrug-resistant and fungal pathogens, and assess in vivo safety and scalability for practical deployment.

REFERENCES

Abdelbaky, A. S., Abd El-Mageed, T. A., Babalghith, A. O., Selim, S., & Mohamed, A. M. (2022). Green synthesis and characterization of ZnO nanoparticles using Pelargonium odoratissimum (L.) aqueous leaf extract and their antioxidant, antibacterial and anti-inflammatory activities. Antioxidants, 11(8), 1444.

Ahmad, S., Munir, S., Zeb, N., Ullah, A., Khan, B., Ali, J., ... & Salman, S. M. (2019). Green nanotechnology: A review on green synthesis of silver nanoparticles - an ecofriendly approach. International Journal of Nanomedicine, 14, 5087-5107.

Amer, M. W., & Awwad, A. M. (2021). Green synthesis of copper nanoparticles by Citrus limon fruits extract, characterization and antibacterial activity. Chemistry International, 7(1), 1-8.

Anand, G. T., Nithiyavathi, R., Ramesh, R., Sundaram, S. J., & Kaviyarasu, K. (2020). Structural and optical properties of nickel oxide nanoparticles: Investigation of antimicrobial applications. Surfaces and Interfaces, 18, 100460.

Anju, T., Parvathy, S., Veettil, M. V., Rosemary, J., Ansalna, T., Shahzabanu, M., & Devika, S. (2021). Green synthesis of silver nanoparticles from Aloe vera leaf extract and its antimicrobial activity. Materials Today: Proceedings, 43, 3956-3960.

Arya, G., Kumari, R. M., Gupta, N., Kumar, A., Chandra, R., & Nimesh, S. (2018). Green synthesis of silver nanoparticles using Prosopis juliflora bark extract: reaction optimization, antimicrobial and catalytic activities. Artificial Cells, Nanomedicine, and Biotechnology, 46(5), 985-993.

Baghayeri, M., Mahdavi, B., Hosseinpor-Mohsen Abadi, Z., & Farhadi, S. (2018). Green synthesis of silver nanoparticles using water extract of Salvia leriifolia: Antibacterial studies and applications as catalysts in the electrochemical detection of nitrite. Applied Organometallic Chemistry, 32(2), e4057.

Balasubramani, S. R., Ewe, L. S., Senthilkumar, S., Narayana Murthy, V., Yew, W. K., Baskaran, R., & Tiong, S. K. (2025). A critical review on green synthesis of copper oxide nanoparticles: characterization and its application in wastewater treatment. Environmental Technology Reviews, 14(1), 797-819.

Chakraborty, N., Banerjee, J., Chakraborty, P., Banerjee, A., Chanda, S., Ray, K., ... & Sarkar, J. (2022). Green synthesis of copper/copper oxide nanoparticles and their applications: a review. Green Chemistry Letters and Reviews, 15(1), 187-215.

Das, P. E., Abu-Yousef, I. A., Majdalawieh, A. F., Narasimhan, S., & Poltronieri, P. (2020). Green synthesis of encapsulated copper nanoparticles using a hydroalcoholic extract of Moringa oleifera leaves and assessment of their antioxidant and antimicrobial activities. Molecules, 25(3), 555.

Dhir, S., Verma, R., Bhatt, S., Garg, V., & Dutt, R. (2023). Green synthesis, characterization, and biomedical applications of copper and copper oxide nanoparticles of plant origin. Current Drug Therapy, 18(5), 391-406.

Eren, A., & Baran, M. (2019). Green synthesis, characterization and antimicrobial activity of silver nanoparticles (AgNPs) from maize (Zea mays L.). Applied Ecology and Environmental Research, 17(2), 4097-4105.

Garibo, D., Borbon-Nunez, H. A., de Leon, J. N. D., Garcia Mendoza, E., Estrada, I., Toledano-Magana, Y., ... & Blanco, A. (2020). Green synthesis of silver nanoparticles using Lysiloma acapulcensis exhibit high-antimicrobial activity. Scientific Reports, 10(1), 12805.

Hafeez, M., Shaheen, R., Akram, B., Haq, S., Mahsud, S., Ali, S., & Khan, R. T. (2020). Green synthesis of cobalt oxide nanoparticles for potential biological applications. Materials Research Express, 7(2), 025019.

Ijaz, F., Shahid, S., Ahmad Khan, S., Ahmad, W., & Zaman, S. (2017). Green synthesis of copper oxide nanoparticles using Abutilon indicum leaf extract: antimicrobial, antioxidant and photocatalytic dye degradation activities. Tropical Journal of Pharmaceutical Research, 16(4), 743-753.

Jamzad, M., & Kamari Bidkorpeh, M. (2020). Green synthesis of iron oxide nanoparticles by the aqueous extract of Laurus nobilis L. leaves and evaluation of the antimicrobial activity. Journal of Nanostructure in Chemistry, 10(3), 193-201.

Kalpana, V., & Devi Rajeswari, V. (2018). A review on green synthesis, biomedical applications, and toxicity studies of ZnO NPs. Bioinorganic Chemistry and Applications, 2018, 3569758.

Khan, M. I., Akhtar, M. N., Ashraf, N., Najeeb, J., Munir, H., Awan, T. I., ... & Kabli, M. R. (2020). Green synthesis of magnesium oxide nanoparticles using Dalbergia sissoo extract for photocatalytic activity and antibacterial efficacy. Applied Nanoscience, 10(7), 2351-2364.

Kombaiah, K., Vijaya, J. J., Kennedy, L. J., Bououdina, M., Ramalingam, R. J., & Al-Lohedan, H. A. (2018). Okra extract-assisted green synthesis of CoFe2O4 nanoparticles and their optical, magnetic, and antimicrobial properties. Materials Chemistry and Physics, 204, 410-419.

Kumar, H., Bhardwaj, K., Kuca, K., Kalia, A., Nepovimova, E., Verma, R., & Kumar, D. (2020). Flower-based green synthesis of metallic nanoparticles: Applications beyond fragrance. Nanomaterials, 10(4), 766.

Letchumanan, D., Sok, S. P., Ibrahim, S., Nagoor, N. H., & Arshad, N. M. (2021). Plant-based biosynthesis of copper/copper oxide nanoparticles: an update on their applications in biomedicine, mechanisms, and toxicity. Biomolecules, 11(4), 564.

Mahdi, M. A., Yousefi, S. R., Jasim, L. S., & Salavati-Niasari, M. (2022). Green synthesis of DyBa2Fe3O7.988/DyFeO3 nanocomposites using almond extract with dual eco-friendly applications: photocatalytic and antibacterial activities. International Journal of Hydrogen Energy, 47(31), 14319-14330.

Mehwish, H. M., Rajoka, M. S. R., Xiong, Y., Cai, H., Aadil, R. M., Mahmood, Q., ... & Zhu, Q. (2021). Green synthesis of a silver nanoparticle using Moringa oleifera seed and its applications for antimicrobial and sun-light mediated photocatalytic water detoxification. Journal of Environmental Chemical Engineering, 9(4), 105290.

Mousavi, S. M., Hashemi, S. A., Ghasemi, Y., Atapour, A., Amani, A. M., Savar Dashtaki, A., ... & Arjmand, O. (2018). Green synthesis of silver nanoparticles toward bio and medical applications: review study. Artificial Cells, Nanomedicine, and Biotechnology, 46(sup3), 855-872.

Naaz, S., Shet, V. B., & Mubarak, N. M. (2024). Green synthesis of copper oxide nanoparticles: Characterization and applications for environmental and biomedical fields. The Canadian Journal of Chemical Engineering, 102(4), 1454-1465.

Pillai, A. M., Sivasankarapillai, V. S., Rahdar, A., Joseph, J., Sadeghfar, F., Rajesh, K., & Kyzas, G. Z. (2020). Green synthesis and characterization of zinc oxide nanoparticles with antibacterial and antifungal activity. Journal of Molecular Structure, 1211, 128107.

Rasheed, T., Bilal, M., Iqbal, H. M., & Li, C. (2017). Green biosynthesis of silver nanoparticles using leaves extract of Artemisia vulgaris and their potential biomedical applications. Colloids and Surfaces B: Biointerfaces, 158, 408-415.

Salayova, A., Bedlovicova, Z., Daneu, N., Balaz, M., Lukacova Bujnakova, Z., Balazova, L., & Tkacikova, L. (2021). Green synthesis of silver nanoparticles with antibacterial activity using various medicinal plant extracts: Morphology and antibacterial efficacy. Nanomaterials, 11(4), 1005.

Saleem, M. H., Ejaz, U., Vithanage, M., Bolan, N., & Siddique, K. H. (2025). Synthesis, characterization, and advanced sustainable applications of copper oxide nanoparticles: a review. Clean Technologies and Environmental Policy, 27(10), 5719-5744.

Siddiqui, M. N., Redhwi, H. H., Achilias, D. S., Kosmidou, E., Vakalopoulou, E., & Ioannidou, M. D. (2018). Green synthesis of silver nanoparticles and study of their antimicrobial properties. Journal of Polymers and the Environment, 26(2), 423-433.

Tailor, G., Yadav, B., Chaudhary, J., Joshi, M., & Suvalka, C. (2020). Green synthesis of silver nanoparticles using Ocimum canum and their anti-bacterial activity. Biochemistry and Biophysics Reports, 24, 100848.

Vasantharaj, S., Sathiyavimal, S., Senthilkumar, P., Kalpana, V., Rajalakshmi, G., Alsehli, M., ... & Pugazhendhi, A. (2021). Enhanced photocatalytic degradation of water pollutants using bio-green synthesis of zinc oxide nanoparticles (ZnO NPs). Journal of Environmental Chemical Engineering, 9(4), 105772.

Velsankar, K., RM, A. K., & Sudhahar, S. (2020). Green synthesis of CuO nanoparticles via Allium sativum extract and its characterizations on antimicrobial, antioxidant, antilarvicidal activities. Journal of Environmental Chemical Engineering, 8(5), 104123.

Vijayaram, S., Razafindralambo, H., Sun, Y.-Z., Vasantharaj, S., Ghafarifarsani, H., Hoseinifar, S. H., & Raeeszadeh, M. (2023). Applications of green synthesized metal nanoparticles - a review. Biological Trace Element Research, 202, 360-386.

Yadi, M., Mostafavi, E., Saleh, B., Davaran, S., Aliyeva, I., Khalilov, R., ... & Panahi, Y. (2018). Current developments in green synthesis of metallic nanoparticles using plant extracts: a review. Artificial Cells, Nanomedicine, and Biotechnology, 46(sup3), 336-343.